Atmos. Chem. Phys. Discuss., 10, 9801–9838, 2010
www.atmos-chem-phys-discuss.net/10/9801/2010/

Atmospheric Chemistry and Physics Discussions

This discussion paper is/has been under review for the journal Atmospheric Chemistry and Physics (ACP). Please refer to the corresponding final paper in ACP if available.

Impact of model resolution on chemical ozone formation in Mexico City; application of the WRF-Chem model

X. Tie[1], **G. Brasseur**[1,2], **and Z. Ying**[3]

[1]National Center for Atmospheric Research, Boulder, CO USA
[2]Climate Service Center, Hamburg, Germany
[3]Department of Earth and Atmospheric Science, York University, Toronto, Canada

Received: 1 April 2010 – Accepted: 8 April 2010 – Published: 16 April 2010

Correspondence to: X. Tie (xxtie@ucar.edu)

Published by Copernicus Publications on behalf of the European Geosciences Union.

Abstract

The resolution of regional chemical/dynamical models has important effects on the calculation of distributions of air pollutants in large cities. In this study, the sensitivity of air pollutants and photochemical O_3 production to different model resolutions is studied by using a regional chemical/dynamical model (version 3 of Weather Research and Forecasting Chemical model – WRF-Chemv3) in Mexico City. The model results with 3, 6, 12, and 24 km resolutions are compared to the surface measurements for CO, NO_x, and O_3. The study shows that the model resolutions with 3 and 6 km have reasonable simulations of surface CO, NO_x, and O_3 concentrations and diurnal variations. The model results intend to underestimate the measurements when the resolution is reduced to 12 km. The calculated surface CO, NO_x, and O_3 concentrations significantly underestimate the measured values at 24 km resolution. This study suggests that 12 km is a threshold resolution for the O_3 and O_3 precursor calculations for using a regional chemical/dynamical model in Mexico City. There are three major factors related to the effects of model resolution on the calculations of O_3 and O_3 precursors, including; (1) the calculated meteorological conditions with different model resolutions, (2) the emission spatial distribution of ozone precursors, and (3) the non-linearly O_3 photochemical productions with different resolutions. Model studies suggest that model resolution (resulting in different meteorological condition and transport process) have larger impacts than emission inventory resolutions for the calculations of O_3 and O_3 precursors. The model calculations show that with coarse resolution of emission inventory (24 km) and fine meteorological condition resolution (6 km), the calculated CO and O_3 are considerably improved compared to the calculation with coarse resolution for both emission inventory and meteorological condition (24 km), suggesting that the impacts of resolution on meteorological condition and transport process are largest for the calculations of O_3 and O_3 precursors. The emission resolution has important effects on the calculation, but the effects are smaller than the model resolution. This study also suggests that the changes of O_3 precursors at different resolutions lead to

ACPD
10, 9801–9838, 2010

important impacts on O_3 chemical formation due to the non-linear relationship between O_3 formation and O_3 precursors. Finally, this study suggests that with the balance between the model performance and required computation time, the 6 km resolution is an optimal resolution for the calculation of O_3 and O_3 precursors in Mexico City.

1 Introduction

In large cities, ozone (O_3) is often a major air pollutant, especially in the industrialized countries. For example, in Houston and the coast cities of California, the ozone concentrations often exceed to 200-300 ppbv (Davis and Speckman, 1999; Lei et al., 2004; Zhang et al., 2004; and Mahmud et al., 2008). Such high ozone concentrations have important effects on human's health (Noyes et al., 2009). High ozone concentrations are photo-chemically produced through a complicated path of photo-chemical process (Crutzen, 1975; Chameides and Walker, 1976; Sillman, 1995; Kleinman et al., 2000). The formation of ozone is-nonlinearly related to the presence in the troposphere of carbon monoxide (CO), nitrogen oxide (NO_x=NO+NO_2), and volatile organic compounds (VOCs). In large cities, these ozone precursors are mainly emitted from anthropogenic activities, i.e., combustion by automobiles energy production and industrial activities. Determination of the spatial distribution of the ozone precursor emissions is always a difficult task, especially in urban areas where high concentrations and variable point sources are present.

In order to better quantify the formation of ozone in large urban areas, numerical chemical/dynamical models are used to assess the path towards high ozone episode events (Lei et al., 2004, 2008; Li et al., 2007; West et al., 2004; Tie et al., 2009a, b; Ying et al., 2009; Zavala et al., 2009a, b; Zhang et al., 2009). However, there are many uncertainties in the calculation of the ozone formation, which is associated with the spatial resolution adapted in these three-dimensional chemical-transport models. The choice of the horizontal resolution adapted in regional chemical/dynamical model has an important impact on the calculated concentrations of ozone and its precursors.

ACPD
10, 9801–9838, 2010

This is explained by the fact that (1) meteorological conditions, which play important roles in distributing ozone and its precursors, changes with model resolutions; (2) emission spatial distribution of the ozone precursor emissions is modified; and (3) due to the strong non-linearly relationship between O_3 and O_3 precursors, differences in O_3 precursor spatial distributions produce different O_3 production rates. These three important problems related to resolution of chemical/dynamical models for calculating ozone formation in large cities are illustrated by a schematic picture (Fig. 1), which lay out clearly the problems we are facing when a chemical/dynamical model is used for studying O_3 photochemistry in large cities.

Model studies at varying horizontal resolutions had performed to study the effects of resolutions on several meteorological parameters. For example, Mass et al. (2002) used a regional dynamical model (MM5- the fifth-generation Pennsylvania State University–National Center for Atmospheric Research Mesoscale Model) to evaluate wind, temperature, and sea level pressure with different model resolution (4, 12, and 36 km). Their result showed that there are significant improvements for calculating these dynamical parameters, especially changing from 36 to 12 km resolution. Colle et al. (2000) used the MM5 model to study precipitation at different model resolution. Their result indicated that the calculated precipitation was noticeable improvement by changing resolution from 36 to 12 km in the model. Cairns and Corey (1998) used the MM5 model to study mountain winds. Their study suggested that the calculated winds were improved by increasing model resolution from 27 to 3 km. In addition to dynamical parameters, previous study was also applied for the impact of model resolutions on predicting fire danger. For example, Hoadley et al. (2004) used the MM5 model to evaluate the model's skill in predicting fire danger at three different resolutions (36, 12, and 4 km). However, their result indicated that little significant improvement was found in skill with increased model resolution, suggesting significant timing and magnitude errors at all resolutions could jeopardize accurate prediction of fire danger.

So far, little attention has been paid to the effects of model resolutions on ozone formation, which involve more complicated scientific issues as mentioned in the above

paragraphs. This study focuses on ozone (O_3) and ozone precursor calculations with various model horizontal resolutions. The model used in this study is a newly developed chemical/dynamical model (version 3 of Weather Research and Forecasting Chemical model – WRF-Chemv3). The WRF-Chem model is used to address scientific questions related to the effects of changing model resolution and emission resolution on O_3 and O_3 photo-chemistry in a mega city (Mexico City). The calculated results are compared to the surface measurements in the city to evaluate the model performance at different resolutions. The paper is organized as follows: In Sect. 2, we describe the regional chemical/dynamical model (WRF-Chem). In Sect. 3, the simulated O_3 and O_3 precursors are compared to the measurement data. Section 4 presents result analysis to determing the effect of the model resolutions on the calculated O_3 distributions and to study the individual contributions from transport, emission, and photochemical processes related to the model resolutions to calculated O_3 and O_3 precursors.

2 Chemical model

An important objective of this study is the intensive use of a regional chemical/dynamical model to study the sensitivity of ozone chemistry to the model emission resolutions. The model used in this study is a recently developed regional chemical/transport model (WRF-Chem, version 3). There are two major parts of the model, i.e., a dynamical model (WRF) and a chemical model (Chem). The Weather Research and Forecasting (WRF) model is a mesocale numerical weather prediction system designed to serve both operational forecasting and atmospheric research needs. The effort to develop WRF has been a collaborative partnership, principally among the National Center for Atmospheric Research (NCAR), the National Oceanic and Atmospheric Administration (NOAA), the National Centers for Environmental Prediction (NCEP), the Forecast Systems Laboratory (FSL), the Air Force Weather Agency (AFWA), the Naval Research Laboratory, Oklahoma University, and the Federal Aviation Administration (FAA). The WRF model is a fully compressible and Euler non-

ACPD
10, 9801–9838, 2010

hydrostatic model. The Yonsei University (YSU) PBL scheme (Hong et al., 2006) is used for calculating PBL height in this study. The detailed description of WRF model can be found in the WRF web-site http://www.wrf-model.org/index.php. In addition to dynamical calculations, a chemical model is coupled on-line with the WRF model (WRF-Chem). A detailed description of WRF-Chem is given by Grell et al. (2005), and is used here with some modifications in the chemical scheme (Tie et al., 2007).

In this study, the model resolutions are selected to be 3, 6, 12, and 24 km in a 900×900 km domain centered on Mexico City. The emission inventory used in this study for SO_2, CO, NO, and VOCs are shown in Table 2 of Tie et al. (2009b). In this model resolution task, the total emissions are the same with different model resolutions, but the horizontal distributions are different due to the different model resolutions (illustrated in Fig. 2). The model runs from 26 March 2006 to 28 March 2006, and only the last day result (28 March 2006) are used (the first two day results are considered as spin up of the model calculations). In previous studies, the WRF-Chem model was evaluated by comparing calculated O_3, CO, and NO_x to the ground measurement from operational monitors in the Mexico City (Tie et al., 2007; Ying et al., 2009; Zhang et al., 2009). The model results showed that the magnitude and timing of simulated diurnal cycles of O_3, CO, and NO_x, and the maximum and minimum O_3 concentrations were generally consistent with surface measurements with 6 km resolution. However, there were also noticeable differences between calculated and measured values (about 10–30%). In this study, the difference between calculated and measured values is further evaluated by considering different model and emission resolutions.

3 Model results

In order to evaluate model performance at different resolutions, modeled results are compared to the surface measurement in Mexico City. Air pollutants in Mexico City have been monitored routinely since 1986 by automatic air quality monitoring network (RAMA) (Molina and Molina, 2002). The measurement site locations are depicted in

Fig. 3 and detailed in Table 1. As indicated in Table 1, there are totally 15 measurement sites, and each site measures different chemical species. For example, the red marked lines show that these measurement sites include only O_3 concentrations; the green marked lines show that these measurement sites include only CO and NO_x concentrations; and the blue marked lines show that these measurement sites include O_3, CO, and NO_x concentrations. On 28 March, the observed noon time wind is from SSW with wind speed of 5–10 m/s and clear sky (Fast 2007). The simulated wind is generally from south with the wind speed of 3–8 m/s at noontime in outside of the city (see Fig. 3). However, inside the city, there is an indication that mountain breeze has strong influences on both the wind directions and speeds. In Table 1, the measurement sites are listed from south to north, except CHA site which is located in far-east location. This site generally has less effect from the city pollutions.

In order to better understand the individual contributions of different processes (such as meteorological condition, transport process, emissions, and non-linear photochemistry) due to changes in horizontal resolutions of the model to the calculations of air pollutants, several chemical species (CO, NO_x, and O_3) are calculated at different resolutions and compared to the measured surface concentrations. For example, the calculated CO concentrations at different resolution are mainly resulted from the changes in meteorological condition, transport process, and emission inventory, but are not resulted from the non-linear photochemistry (CO has a slow chemistry reaction rate). By contrast, O_3 is a strong photochemical active species, and is strongly controlled by non-linear photochemistry due to changes in horizontal resolution. As a result, comparisons for different characterizations of chemical oxidants can show some insights of the contributions from different processes to different chemical species due to changes in horizontal resolutions.

Figure 4 shows the calculated surface CO distribution at different resolutions. It shows that the surface CO has generally the same horizontal pattern at 3, 6, 12, and 24 km resolutions. The surface CO concentrations have highest concentrations in center of city, and are transported northward with apparent downwind plumes. How-

ACPD
10, 9801–9838, 2010

ever, there are apparently different in detailed horizontal structures. The maximum CO concentrations are higher with high resolutions (3 and 6 km), and decrease sharply with lower resolutions (12 and 24 km). For example, the maximum concentrations are 2000–3000 ppbv at center of the city with 3 and 6 km resolutions. The maximum concentrations decrease to 1000–1500 ppbv at center of the city with 12 km resolution, and further decrease to 700 ppbv with 24 km resolution. At lower resolution, the CO concentrations are more diffused than the CO concentrations at higher resolution. For example, the high CO concentration has relatively fine structure in the center of the city at 3 or 6 km resolution. By contrast, the high concentration of CO at 24 km is more uniformly distributed in the city. There is also noticeable feature that the high CO concentration is shift northward of the city at 24 km resolution due to the coarse resolution of emission (see Fig. 2). The diffusion of high concentrations coupling with the northward shift has important impacts on the calculated surface concentrations of CO and O_3 as shown in the following sections.

Figure 5a shows the measured and calculated diurnal variations of surface CO concentrations at the measurement sites. The result suggests that there are 2 maxima and 2 minima in both the measurements and the calculations. The first maximum of CO occurs around 8 a.m. and second happens in late evening. The first minimum of CO occurs around noon time and the second happens in the early morning. As explained by Tie et al. (2007), this strong diurnal variation is mainly due to the combination of diurnal variations of PBL (Planetary Boundary Layer) height and emission of CO. The calculated diurnal variations have similarity compared to the measured variations. However, some distinguished differences are noticeable between the measured and calculated values, especially for the lower resolution (24 km) results. The results for 3 and 6 km resolutions have generally similar results and are close to the measured values, except that the evening maximum is somewhat different between 3 km and 6 km resolutions. For the 12 km resolution, the calculated CO diurnal variation is similar to the results of 3 and 6 km. However, the magnitude of the morning maximum is smaller than the results of 3 and 6 km, and in some sites (SUR, PED, LAG, and HAN) the calculated morning

maximum at 12 km resolution is underestimated the measured values. As indicated in Figs. 2 and 3, these sites are located in the center of the city with highest emission rate. As a result, the lower emission resolution (12 km) causes dilution of the calculated CO in these sites, leading to underestimation of the calculated CO concentrations. However, in north side of the city (TLA, SAG, TLI, and VIF), the calculated CO at 12 km resolution is very similar to the calculated CO with 3 and 6 km resolution. At 24 km resolution, the calculated CO concentrations have a significant changes compared to the calculation at 3 and 6 km, and largely underestimate the measured values. In the center of city sites (SUR, PED, PLA, and LAG), the calculated CO concentrations are close to background value (100 ppbv) and no diurnal variation is apparent, suggesting that this coarse resolution is not suitable for the model calculation in the center of the city. In the north edge of the city sites (SAG, TLA, TLI, and VIF), the calculated CO concentrations are much improved compared to the city center sites, especially at VIF site (far-north of the city and downwind of city plume), indicating that in the edge of the city, the coarse resolution has better calculation than the center of the city.

Figure 5b shows the measured and calculated diurnal variations of surface NO_x concentrations at the measurement sites. The result suggests that the NO_x calculations at different resolutions have similar diurnal variations to the CO calculations. The main conclusion is that the calculated NO_x concentrations are generally consistent with the measured NO_x diurnal variation at 3, 6, and 12 km. However, at 24 km resolution, the calculated NO_x diurnal changes sharply, and the calculated NO_x significantly underestimates the measured values, especially in the center of the city sites. In the north edge of the city sites, the calculated NO_x concentrations at coarse resolutions are improved compared to the city center sites, especially at VIF site. Because both CO and NO_x are directly emitted from the surface sources, the calculation nearby the city sites is largely dependent upon the resolution of emission inventory. There is an indication that the 24 km resolution for emission and model is too coarse to apply the regional model for studying the detailed distributions in Mexico City.

Figure 5c shows the measured and calculated diurnal variations of surface O_3 concentrations at the measurement sites. Unlike CO and NO_x which are directly emitted from surface sources, O_3 is photochemically formed and the chemical formation of O_3 has complicated non-linear relationship with O_3 precursors (CO, NO, and VOCs). As a result, the different distributions of O_3 precursors (such as CO and NO_x) resulted from the different resolutions have important impacts on O_3 distributions. The calculated O_3 diurnal variations suggest that the O_3 concentrations at 3 and 6 km resolutions have a strong maximum in the afternoon, and the maximum is comparable to the measured O_3 maximum. There is also an indication that at the center of the city (TAC, HAN, and TLA), the calculated O_3 maximum overestimates the measured O_3 values. The calculated O_3 minimum occurs in the morning at 3, 6, and 12 km resolutions, which is consistent with the measured minimum. However, the calculated O_3 concentrations at 24 km resolution are very different compared to the measured result, showing smaller diurnal variations. The maximum of O_3 in the afternoon is significantly underestimated in the downwind city and city center sites. The minimum in the morning is largely overestimated in these sites. In the downwind and edge of the city sites (such as CHA and CUA sites), the O_3 diurnal variations are better calculated than in the center of city.

Figure 6 shows that the mean diurnal variations of CO, NO_x, and O_3 averaged from all measurement sites. The result suggests that the calculated NO_x diurnal variations are generally consistent with the measured values at resolutions of 3, 6, and 12 km. During the early morning the measure NO_x concentrations are about 30 ppbv, and the calculated concentrations at 3 and 6 km resolution are slightly overestimated the measured values. At 8 a.m., the measured NO_x concentrations increase rapidly, reaching a maximum of 160 ppbv. In comparison, the calculated NO_x maximum (140 ppbv) is close to the measured maximum at 3 and 6 km resolutions. During daytime, the measured NO_x concentrations are reduced to a minimum of 40 ppbv, resulting mainly from a rapid increase in the PBL height (Tie et al., 2007). The calculated NO_x with 3, 6, and 12 km resolutions are also rapidly decreased from the morning maximum to the minimum. At 24 km resolution, there is a very weak diurnal variation and the calculated NO_x

ACPD
10, 9801–9838, 2010

concentrations are consistently lower than the measured values, especially during the morning maximum. For example, the calculated morning maximum is about 30 ppbv, which is approximately 80% lower than the measured maximum (160 ppbv). The calculated mean CO diurnal variation has similar features with the calculated mean NO_x. In general, the calculated CO concentrations at 24 km resolution have significantly underestimated the measured values, especially during the morning maximum.

The averaged O_3 diurnal variation (shown in the lower panel of Figure 6) is very different compared to the averaged CO and NO_x diurnal variations. There is a minimum in the morning (at 7 a.m.) and a maximum in the afternoon (at 14 p.m.). The calculated O_3 concentrations at 3, 6, and 12 km have a similar diurnal variation. However, the calculated O_3 concentrations at 3 km resolution are higher than the measured values, especially in the afternoon maximum (by about 35%). By contrast, the calculated O_3 diurnal variation at 24 km resolution is very different compared with the measured diurnal variation. The calculated O_3 concentrations during daytime (from 8 a.m. to 19 p.m.) are consistently lower than the measured values. For example, at 14 p.m., the calculated O_3 concentration is 45 ppbv which is about 45% lower than the measured value (80 ppbv). The calculated O_3 concentrations during nighttime (from 18 p.m. to 7 a.m.), are consistently higher than the measured values. Because the O_3 diurnal variation is strongly regulated by O_3 precursors in large cities (Zhang et al., 2004), the smaller O_3 diurnal variation at 24 km resolution suggest the O_3 precursors are underestimated in the city region, which is consistent to the calculated results of CO and NO_x indicated in the upper and middle panels of Fig. 6.

The above results clearly indicate that there is a threshold value for the model resolution in calculating O_3 and O_3 precursors in regional chemical/dynamical models. At the threshold resolution, the model is unable to adequately describe the air pollutant distributions in large cities. In our study, the calculated results from 12 km to 24 km show strong changes for CO, NO_x, and O_3 concentrations. The results at 24 km show considerable differences compared to the measured results, and are not suitable for calculating the distributions of air pollutants in Mexico City. At 12 and 24 km resolu-

tions, the ratios of the city range (about 70 km in length and width) to each horizontal grid length are about 6 to 1 and 3 to 1. This result suggests that the threshold value for the model resolution is 12 km, which implying that the ratio between range of city and grid length of models is about 6 to 1. However, this threshold value may only be suitable for Mexico City, and need to be further tested in other large cities.

4 Discussions of results

The above study indicates that the model resolution has very strong impacts on the calculated O_3 and O_3 precursor concentrations, and there is a threshold value for the resolution of chemical/dynamical models when they are applied in calculating the distributions of air pollutants in large cities. As we illustrated before (shown in Fig. 1), the impacts of model resolutions on the calculated O_3 and O_3 precursor calculations can be attributed to the 3 main factors; (1) the emission spatial distributions of ozone precursors, (2) the calculated meteorological parameters associated with transport process at different model resolutions, and (3) the non-linearly photochemical between O_3 and O_3 precursors. In order to study the individual contribution of the above 3 factors to the calculated results, 5 model runs are conducted and are listed in Table 2. In the table, the Run-1 through Run-4 changes model resolutions from 3 to 24 km, and the changes in the calculated O_3 and O_3 precursors are due to the combination of all 3 factors. The individual contributions due to the 3 factors cannot be separated from the results. Thus, the Run-5 is designed to separate the 3 factors. In the Run-5, the model contains 6 km resolution, but emission resolution is averaged to be 24 km resolution. As a result, the difference between Run-5 and Run-2 is mainly due to the difference of emission resolutions, and the difference between Run-5 and Run-4 is mainly due to the difference of resolutions of the calculated meteorological conditions and photochemistry.

ACPD
10, 9801–9838, 2010

4.1 The effects of meteorological conditions at different resolutions

Figure 7 shows the calculations of CO surface distributions for the 3 cases (Run-2, Run-4, and Run-5). Because CO is a relatively chemical inactive species in a short time scale (a few days), the calculated CO distributions are only affected by the resolutions of transport processes (driven by the calculated meteorological conditions, such as wind direction and speed) and emission inventory. As shown in Fig. 7, there are very large differences between Run-5 and Run-4, suggesting that the transport processes at different resolutions have significant effects for the calculated CO distributions. For example, the calculated wind pattern in Run-4 is in a coarse distribution and the detailed wind distributions shown at 6 km resolution (Run-5) cannot be calculated in the calculation in Run-4. There are also indications that the mountain breeze in west and east edge of Mexico City is shown at 6 km resolution, but cannot be calculated in 24 km resolution. These detailed wind distributions play important roles in distributing the CO which emitted from the city sources. In addition, the calculated CO concentrations at the 24 km resolution tend to be diluted or averaged in the large grid area (576 km^2), leading to reduce CO concentrations in the center of city and enhance CO concentrations in the outside of the city area (see Fig. 7).

4.2 The effects of emission inventory at different resolutions

As shown in Table 2, for Run-2 and Run-5, both the model resolutions are at 6 km except that the emission inventories are different (6 km in Run-2 and 24 km in Run-5). As a result, the calculated CO is mainly due to the different emission resolutions. The result in Fig. 7 shows that the calculations of CO surface distributions of Run-5 are considerably improved compared to the result of Run-4, suggesting that the improvement in meteorological conditions associated with transport process lead to more detailed CO distributions in center of the city. However, there are also clear differences between Run-2 and Run-5. This suggests that the resolution at which the emissions are provided, has also a significant impact on the calculated CO distributions. For example,

ACPD
10, 9801–9838, 2010

the maximum of CO in the center of city is reduced from 1000 to 700 ppbv, when higher resolution emissions are adopted. There are also indications that the CO distributions obtained with Run-5 are more diffusive than with Run-2. However, the changes in the atmospheric resolution of dynamics and photochemistry appear to affect the model results more substantially than when the resolution of surface emissions is increased. As shown by Fig. 8, the CO calculations with the fine model resolution (6 km) and the coarse resolution of emissions (24 km) improved CO diurnal variations, especially in the sites at the center of the city (such as SUR, PED, PLA, and LAG), but still underestimate the measured values at other sites (such as HAN and SAG).

4.3 The effects of ozone photochemistry

As we described above, ozone is not directly emitted from surface sources, but is closely related to O_3 precursors (including CO, NO_x, and VOCs). Thus, the calculated O_3 distributions are not directly dependent upon the resolution of the emission inventories, but are indirectly related to the resolution of precursor emissions. Because the ozone formation rate is a nonlinear function of O_3 precursors (Lin et al., 1988; Kleinman, 2000), the chemical production rate of ozone is a function of model resolution.

In order to get insights of the effects of resolution on ozone photochemistry, ozone chemical productions are calculated for Run-2, Run-4, and Run-5. The ozone chemical production is initiated by the oxidization of CO and VOCs, which leads to the production of HO_2 and RO_2 radicals. In the presence of NO, ozone is produced by the following reaction chain (Brasseur et al., 1999):

$$HO_2 + NO \rightarrow NO_2 + OH \quad \text{(R1)}$$

$$RO_2 + NO \rightarrow NO_2 + RO \quad \text{(R2)}$$

$$NO_2 + h\nu \rightarrow NO + O \quad \text{(R3)}$$

$$O + O_2 \rightarrow O_3 \quad \text{(R4)}$$

From Reactions (R1) and (R4), the O_3 chemical production rate is expressed by

$$P(O_3) = (P_{HO_2}(O_3) + P_{RO_2}(O_3)) \quad (1)$$

$$P_{HO_2}(O_3) = (k_1 \times (HO_2)(NO)) \quad (2)$$

$$P_{RO_2}(O_3) = (\Sigma k_{2i} \times (RO_2)_i(NO)) \quad (3)$$

where $P(O_3)$ represents the total rate of O_3 production and $P_{HO_2}(O_3)$ and $P_{RO_2}(O_3)$ the rate of O_3 production due to the oxidation of NO, HO_2 and RO_2, respectively. Note that RO_2 stands for several types of peroxy radicals that produced by the oxidation by the OH radical of VOCs. The parameters of k_1, and k_{2i} are the rate coefficients for Reactions (R1) and (R2), respectively.

Figure 9 shows the calculated noontime rate of ozone photochemical production ($P(O_3)$) (ppbv/hour) with Run-1, Run-2, Run4, and Run-5, respectively. These graphs show that the distribution of $P(O_3)$ is generally similar for Run-1 and Run-2 with a maximum value of 50–60 ppbv/hour at the center of the city. However, it appears that the O_3 distribution of Run-1 has a finer structure than in the case of Run-2 due to the finer resolution of the model. The distribution of $P(O_3)$ produced by Run-4 is very different than in Run-1 and Run-2, highlighting that the coarse resolution (24 km) is not suitable for applying ozone chemical study in urban area. The calculated $P(O_3)$ has a maximum (30–40 ppbv/hour) in northwestern area of the city instead of in the center of the city (as shown in Run-1 and Run-2). As a result, the calculated O_3 diurnal variations are close to the measured values in these sites (such as HAN, SAG, and CHA), but are largely underestimated when compared to the values measured in the center of the city, and in the southern area (such as TPN, TAH, PED, and TAX). At these sites, the calculated ozone production rates are very low, and the afternoon O_3 concentration maxima are significantly underestimated when compared to the measured diurnal variations (see Fig. 9). The result of Run-4 also suggests that the calculated ozone production is diluted outside the city due to the large grid cell (576 km^2). For example, at the west edge of the city, the ozone production rate is about 10–15 ppbv/hour in

Run-5, while the values are less than 5 ppbv/hour in the finer resolution calculations (Run-1 and Run-2).

The calculated O_3 production is considerably improved in Run-5 compared to Run-4, even though both calculations use the same spatial resolution for the surface emission rate (24 km). However, with the finer grid resolution of Run-5 the distribution of $P(O_3)$ is similar to the results of Run-1 and Run-2. The $P(O_3)$ maximum in the center of the city is about 50–60 ppbv/hour, which is similar to the values provided by Run-1 and Run-2. As a result, the calculated O_3 diurnal variation is also considerably improved compared to the measured values. In this case, the diurnal variation in ozone concentration is better represented, especially at the southern and city sites (TPN, TAH, PED and TAX). The ozone diurnal variation derived in Run-4 is significantly underestimated at these sites (see Fig. 10).

4.4 Overall discussion

In order to gain some integrated insights of the effects of model resolution on the calculated CO, NO_x, and O_3 concentrations, the measured and calculated CO, NO_x, and O_3 concentrations are averaged at all sites as shown in Fig. 11. The upper panel shows that the mean measured NO_x concentration is 60 ppbv, which is close to the calculated NO_x concentrations preferment at 3 and 6 km resolution. The averaged NO_x concentration calculated at 12 km resolution is lower than the measured value, but the averaged NO_x concentration obtained at 24 km resolution is significantly lower (70%) than the measured value. It appears therefore that 12 km is a threshold resolution for the calculation of NO_x distribution in Mexico City. The calculation with a coarse emission inventory (24 km) and a fine model resolution (6 km) has significantly improvement for the calculated NO_x concentrations, but has slightly underestimation of the measured NO_x concentration.

The averaged CO concentrations (middle panel) are characterized by features that are similar to those of the average NO_x concentrations. The model shows that the calculated CO concentrations at 3 and 6 km resolution are most representative of the

measured values. The average CO concentration at 12 km resolution is lower than the measured value, while the average NO_x concentration at 24 km resolution is significantly lower than the measured value. This result confirms that 12 km resolution is the threshold value for the calculation of CO distribution in Mexico City.

Ozone chemistry is very different during daytime and nighttime (Sillman, 1995; Zhang et al., 2004). As a result, the O_3 concentrations are separately averaged for daytime (8 a.m to 19 p.m.) and nighttime (20 p.m. to 7 a.m.). The mean measured O_3 daytime concentration is about 45 ppbv, which is close to the calculated O_3 concentrations at 6 and 12 km resolution. The calculated O_3 concentration at 3 km resolution overestimates the measured value. The average daytime ozone density at 24 km resolution is lower than the measured value by about 35%. Interestingly, the measured ozone concentrations are characterized by a very large difference (30 ppbv) between the daytime and nighttime values. The calculated O_3 concentrations with 3, 6, and 12 km also exhibit a large daytime to nighttime difference. This difference, however, is limited to only 6 ppbv when a 24 km is adopted for the model resolution. The small difference between day and night for this resolution suggests both the day and night O_3 chemistries cannot be well calculated, resulting in a poorly calculated O_3 diurnal variation at 24 km resolution. The main reason is that ozone formation is strongly regulated by NO_x concentrations, which is not reasonably simulated at 24 km. This is a further confirmation that the threshold resolution for the calculation of O_3 is at 12 km.

Regional chemical/dynamical models (such as the WRF-Chem model) requires a large amount computation time, which often exceeds the capability for some computers. The reduction of model grid points (decreasing model resolution) can reduce the computation time of models. As indicated from Fi. 13, increasing the grid points from 24 km resolution to 3 km resolution leads to the increase of computation time by 512 times. However, increasing the grid points from 24 km resolution to 6 km resolution only requires 64 times more computation time. From the above analysis, the threshold resolution is at 12 km. With the balance between the model performance and required computation time, the 6 km resolution is considered as an optimal resolution for the

ACPD
10, 9801–9838, 2010

calculation of O_3 and O_3 precursors in Mexico City.

5 Summary

The effects of model resolutions (including grid resolution and emission inventory resolutions) on the calculated CO, NO_x, and O_3 distributions are studied by using the WRF-Chem chemical/dynamical model in Mexico City. This study is focused on the 3 major issues regarding the impacts of model resolutions on the calculations of O_3 formation; (1) the calculated meteorological conditions changes due to different model resolutions, (2) the different resolutions of emission spatial distributions of ozone precursors, and (3) the non-linearly O_3 photochemical productions due to different resolutions. In this study, 5 model calculations are performed to study the above effects, including Run-1 (3 km resolution), Run-2 (6 km resolution), Run-3 (12 km resolution), Run-4 (24 km resolution), and Run-5 (6 km grid resolution with 24 km emission inventory resolution). The results suggest that the model resolutions have important effects on the calculations of O_3 and O_3 precursors in Mexico City. The calculated CO, NO_x, and O_3 surface concentrations are reasonably simulated the measured distributions in Mexico City at 3 and 6 km resolutions. The calculated results show some underestimations at 12 km resolution. When the model resolution changes to 24 km, the model performance are very poor compared to the measured values in Mexico City, suggesting that there is a threshold value for model resolution for the calculations of O_3 and O_3 precursor for regional chemical/dynamical models. In our case, the suggested threshold value is 12 km. When model resolution is lower than the threshold resolution, the calculated results are very different compared to the measured distributions for O_3 and O_3 precursors. The ratio of the city range (about 70 km in length and width) to threshold resolution is 6 to 1, and this ratio can be considered as a threshold model resolution for other cities in general. However, for each individual large city, model calculations should be performed to study the threshold resolutions.

The sensitivity studies suggest that the largest impacts of the changes in model resolutions on the calculated O_3 and O_3 precursors are due to the changes in meteorological conditions and the transport processes. The changes in emission resolutions have modest impact on the model calculations. Finally, this study suggests that the changes of O_3 precursors at different resolutions lead to important impacts on O_3 chemical formation due to the non-linear relationship between O_3 formation and O_3 precursors.

Acknowledgements. The authors would like to thank George Grell and Steve Peckham at NOAA for providing us with the WRF-Chem model. We wish to thank Jim Greenburg for helpful discussions. The National Center for Atmospheric Research is sponsored by the National Science Foundation.

References

Brasseur, G., Orlando, J., and Tyndall, G.: Atmospheric Chemistry and Global Change, Oxford University Press, 1999.

Cairns M. M. and Corey, J.: An application of the MM5 to modeling high winds in complex terrain: A case study in the eastern Sierra. Western Region Tech. Attachment 98-13, 4 pp., 1998.

Chameides, W. L. and Walker, J.: Time dependent photochemical model for ozone near the ground, J. Geophys. Res., 81, 413–420. 1976.

Colle, B. A., Mass, C. F., and Westrick, K. J.: MM5 precipitation verification over the Pacific Northwest during the 1997–1999 cool seasons, Wea. Forecasting, 15, 730–744, 2000.

Crutzen, P. J.: Physical and chemical processes which control the production, destruction, and distribution of ozone and some other chemically active minor constituents, GARP Publications Series, 16, 236–243. 1975.

Davis, J. M. and Speckman, P,: A model for predicting maximum and 8 h average ozone in Houston, Atmos. Environ., 33, 2487–2500. 1999.

Fast, J. D., de Foy, B., Acevedo Rosas, F., Caetano, E., Carmichael, G., Emmons, L., McKenna, D., Mena, M., Skamarock, W., Tie, X., Coulter, R. L., Barnard, J. C., Wiedinmyer, C., and Madronich, S.: A meteorological overview of the MILAGRO field campaigns, Atmos. Chem.

Phys., 7, 2233–2257, 2007, http://www.atmos-chem-phys.net/7/2233/2007/.
Grell, G. A., Peckham, S. E., Schmitz, R., McKeen, S. A., Wilczak, J., and Eder, B.: Fully coupled "online" chemistry within the WRF model, Atmos. Environ. 39, 6957–6975, 2005
Hoadley, J. L., Westrick, K., Ferguson, S. A., Goodrick, S. L., Bradshaw, L., and Werth, P.: The Effect of Model Resolution in Predicting Meteorological Parameters Used in Fire Danger Rating, J. Appl. Meteoro., 43, 1333–1347, 2004.
Kleinman, L. I., Daum, P. H., Imre, D. J., Lee, J. F., Lee, Y.-N., Nunnermacker, L. J., Springston, S. R., Weinstein-Lloyd, J., and Newman, L.: Ozone production in the New York City urban plume, J. Geophys. Res., 105, 14495–14512, doi:10.1029/2000JD900011, 2000.
Lei, W., Zhang, R., Tie, X., and Hess, P.: Chemical characterization of ozone formation in the Houston-Galveston area, J. Geophys. Res., 109, D12, doi:10.102/2003JD004219, 2004.
Lei, W., Zavala, M., de Foy, B., Volkamer, R., and Molina, L. T.: Characterizing ozone production and response under different meteorological conditions in Mexico City, Atmos. Chem. Phys., 8, 7571–7581, 2008, http://www.atmos-chem-phys.net/8/7571/2008/.
Li., G., Zhang, R., Fan, J., and Tie, X.: Impacts of biogenic emissions on photochemical ozone formation in Houston, Texas, J. Geophys. Res., 112, D10309, doi:10.1029/2006JD007924, 2007.
Lin, X., Trainer, M., Liu, S. C.: On the nonlinearity of the tropospheric ozone production, J. Geophys. Res., 93(D12), 15879–15888, doi:10.1029/88JD03750, 1988.
Mahmud, A, Tyree, M., Cayan, D., Motallebi, N., Kleeman, M., and Michael J.: Statistical downscaling of climate change impacts on ozone concentrations in California, J. Geophys. Res. 113, D21103, doi:10.1029/2007JD009534, 2008.
Mass C. F., Ovens, D., Westrick, K., and Colle, B. A.: Does increasing horizontal resolution produce more skillful forecasts?, B. Am. Meteor. Soc, 83, 407–430, 2002.
Molina, L. and Molina, M.: Air Quality in the Mexico MegaCity: An Integrated Assessment, Kluwer Academic Publishers, Dordrecht, 2002.
Noyes, P. D., McElwee, M. K., Miller, H. D., Clark, B. W., Van Tiem, L. A., Walcott, K. C., Erwin, K. N., and Levin, E. D.: The toxicology of climate change: Environ. Int., 35, 971–986, 2009.
Sillman, S.: The use of NOy, H_2O_2, and HNO_3 as indicators for ozone-NO_x-hydrocarbon sensitivity in urban locations, J. Geophys. Res., 100, 14175–14188, 1995.
Tie, X, Madronich, S., Li, G. H., Ying, Z., Zhang, R., Garcia, A., Lee-Taylor, J., and Liu, Y.:

Characterizations of chemical oxidants in Mexico City: A regional chemical/dynamical model (WRF-Chem) study, Atmos. Environ., 41, 1989–2008, 2007.

Tie, X., Geng, F. H., Peng, L., Gao, W., and Zhao, C. S.: Measurement and modeling of O_3 variability in Shanghai, China; Application of the WRF-Chem model, Atmos. Environ., 43, 4289–4302, 2009a.

Tie, X., Madronich, S., Li, G., Ying, Z., Weinheimer, A., Apel, E., and Campos, T.: Simulation of Mexico City plumes during the MIRAGE-Mex field campaign using the WRF-Chem model, Atmos. Chem. Phys., 9, 4621–4638, 2009b, http://www.atmos-chem-phys.net/9/4621/2009/.

West, J., Zavala, J., Molina, M. A., Molina, L. T., Martini, M. J., McRae, F. S., Iglesias, G. J., and Colina, G. S.: Modeling ozone photochemistry and evaluation of hydrocarbon emissions in the Mexico City metropolitan area. J. Geophys. Res., 109, D19312, doi:10.1029/2004JD004614, 2004.

Ying, Z., Tie, X., and Li, G. H.: Sensitivity of ozone concentrations to diurnal variations of surface emissions in Mexico City: A WRF/Chem modeling study, Atmos. Environ, 43, 851–859, 2009.

Zavala, M., Lei, W., Molina, M. J., and Molina, L. T.: Modeled and observed ozone sensitivity to mobile-source emissions in Mexico City, Atmos. Chem. Phys., 9, 39–55, 2009a

Zavala, M., Herndon, S. C., Wood, E. C., Onasch, T. B., Knighton, W. B., Marr, L. C., Kolb, C. E., and Molina, L. T.: Evaluation of mobile emissions contributions to Mexico City's emissions inventory using on-road and cross-road emission measurements and ambient data, Atmos. Chem. Phys., 9, 6305–6317, 2009b, http://www.atmos-chem-phys.net/9/6305/2009/.

Zhang, R., Lei, W., Tie, X., and Hess, P.: Industrial emissions cause extreme diurnal urban ozone variability, Proceedings of National Academic Science USA, 101, 6346–6350, 2004.

Zhang, Y., Dubey, M. K., Olsen, S. C., Zheng, J., and Zhang, R.: Comparisons of WRF/Chem simulations in Mexico City with ground-based RAMA measurements during the 2006-MILAGRO, Atmos. Chem. Phys., 9, 3777–3798, 2009, http://www.atmos-chem-phys.net/9/3777/2009/.

Table 1. The information of surface measurement sites in Mexico City for O_3, CO, and NO_x.

Sites	Lon	Lat	Name	Measured Spec.
1	−99.01	19.25	TAH	O_3
2	−99.18	19.26	TPN	O_3
3	−99.15	19.31	SUR	CO, NO_x
4	−99.20	19.33	PED	O_3, CO, NO_x
5	−99.12	19.34	TAX	O_3
6	−99.30	19.36	CUA	O_3
7	−99.20	19.37	PLA	CO, NO_x
8	−99.08	19.42	HAN	O_3, CO, NO_x
9	−99.14	19.44	LAG	O_3, CO, NO_x
10	−99.20	19.45	TAC	O_3, CO, NO_x
11	−99.20	19.53	TLA	CO, NO_x
12	−99.03	19.53	SAG	O_3, CO, NO_x
13	−99.18	19.60	TLI	CO, NO_x
14	−99.10	19.66	VIF	CO, NO_x
15	−98.90	19.47	CHA	O_3

The reds represents for O_3 measurement only; the yellows for CO and NO_x only; and the blues for O_3, CO, and NO_x.

ACPD
10, 9801–9838, 2010

Table 2. The information regarding the model runs at different resolutions.

	Resolution	Note
Run-1	3 km	Emission (3 km) and Grid (3 km)
Run-2	6 km	Emission (6 km) and Grid (6 km)
Run-3	12 km	Emission (12 km) and Grid (12 km)
Run-4	24 km	Emission (24 km) and Grid (24 km)
Run-5	6 km	Emission (24 km) and Grid (6 km)

ACPD
10, 9801–9838, 2010

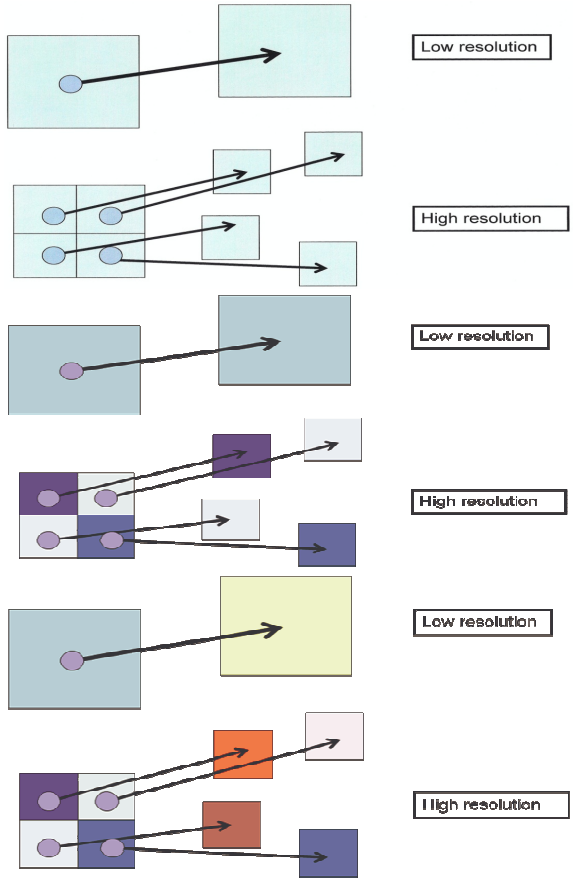

Fig. 1.

ACPD
10, 9801–9838, 2010

Fig. 1. Schematic representation of the different processes by which the horizontal resolution of a chemical transport model affects the calculated concentration of reactive compounds such as ozone in the vicinity of large urban areas: (1) Impact of resolution on the calculation of meteorological quantities and transport of air pollutants (upper panel). This panel indicates that the result of meteorological condition at higher horizontal resolution intends to transport air pollutants in different locations in compared to the result at lower resolution. (2) Impact of resolution on the calculation of meteorological conditions with changes in emission inventory resolutions (model panel). This panel illustrates that in addition to transporting in different locations as the above panel, the uniformed emission distribution at high resolution can result in more uniformed distribution of air pollutants than the distribution of lower resolution emission case. (3) The impact of resolutions on the calculations of meteorological conditions with changes in emission inventory resolutions and non-linear photochemistry (lower panel). This panel suggests that the non-linear chemistry adds more uniformed distribution for air pollutants (such as ozone) at high resolution case than lower resolution.

ACPD
10, 9801–9838, 2010

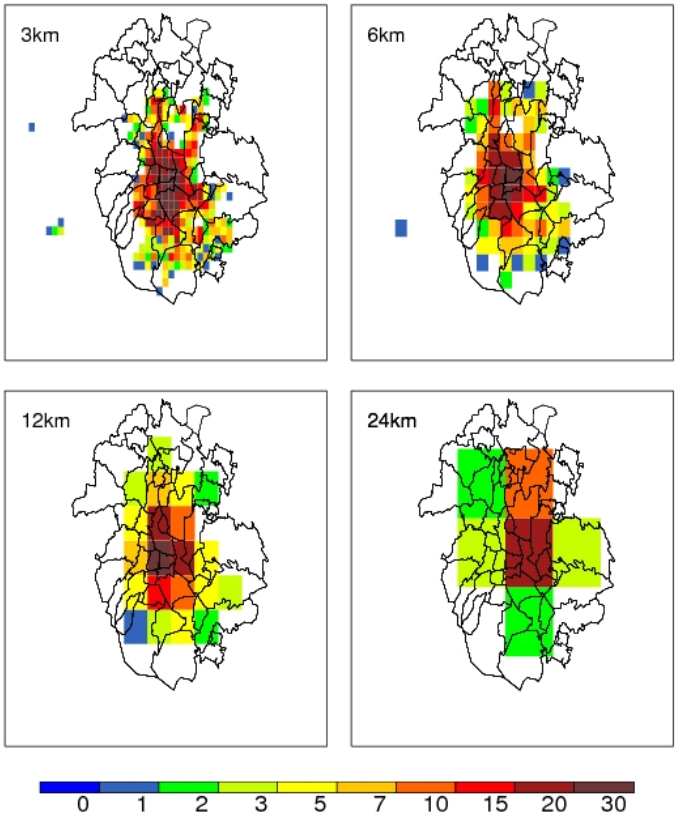

Fig. 2. Emission inventory of carbon monoxide in Mexico City at different resolutions; **(a)** $3\times3\,km^2$, **(b)** $6\times6\,km^2$, **(c)** $12\times12\,km^2$, and **(d)** $24\times24\,km^2$.

ACPD
10, 9801–9838, 2010

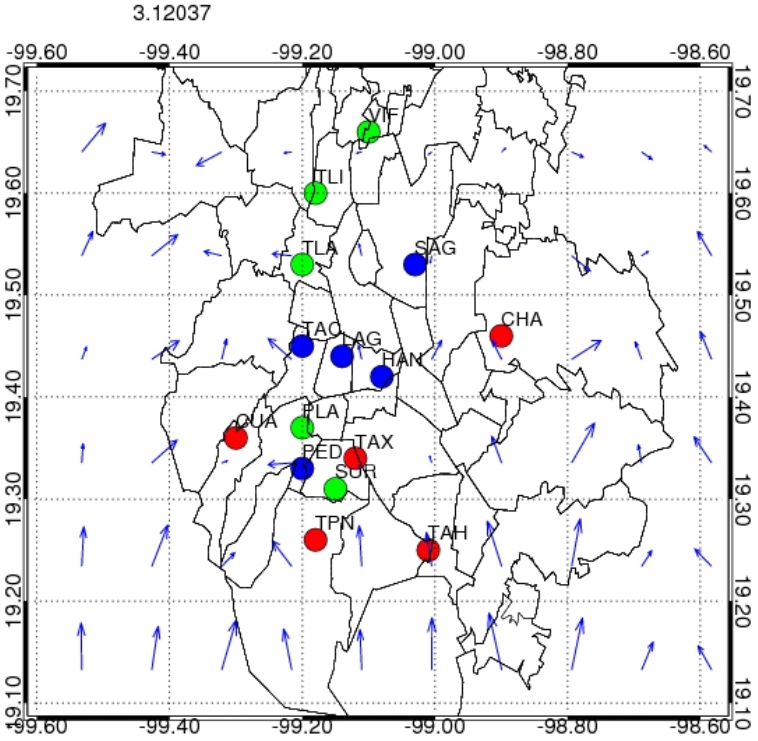

Fig. 3. Surface measurement sites in Mexico City. The red dots represent sites for only ozone measurements; the green dots represent the sites when CO and NO_x are measured; and the blue dots represent the sites when CO, NO_x, and O_3 are measured. The calculated wind pattern at 12 p.m. on 28 March 2006 is also shown.

ACPD
10, 9801–9838, 2010

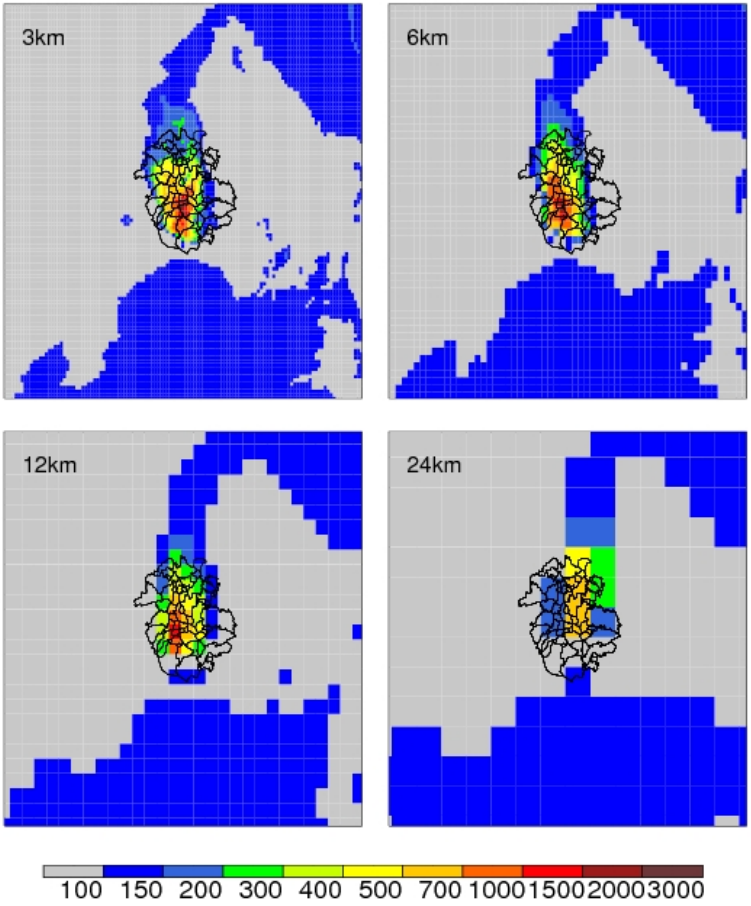

Fig. 4. Calculated CO surface mixing ratio (ppbv) at different resolutions in Mexico City, including; **(a)** 3×3 km^2, **(b)** 6×6 km^2, **(c)** 12×12 km^2, and **(d)** 24×24 km^2.

ACPD
10, 9801–9838, 2010

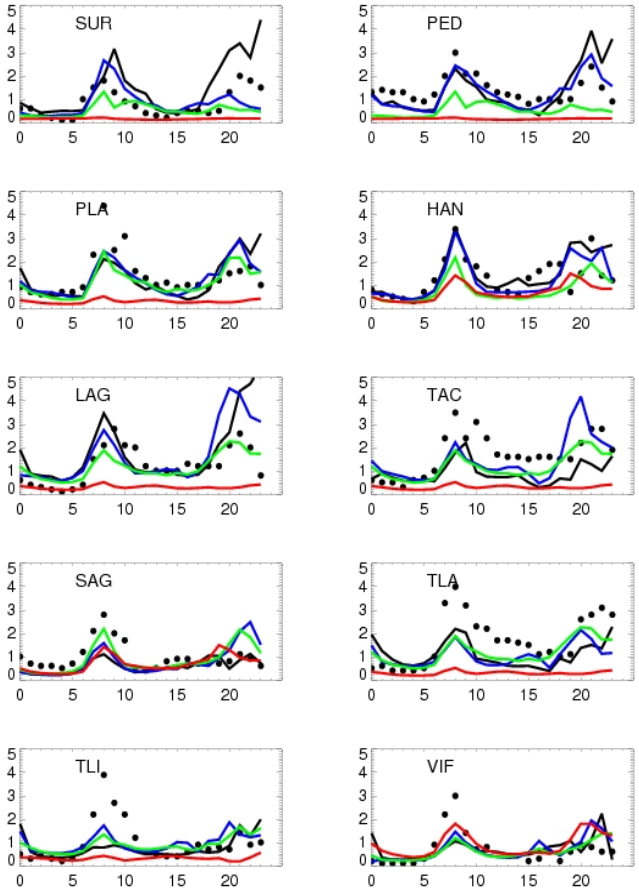

Fig. 5a. Calculated and measured surface diurnal variations for CO mixing ratio (ppmv) at various sites of Mexico City (shown in Table 1) in the different resolutions. Black lines represent the calculated value at 3 km resolution; blue lines for 6 km resolution; green lines for 12 km resolution, red lines for 24 km resolution. Black dots represent the measured values.

ACPD
10, 9801–9838, 2010

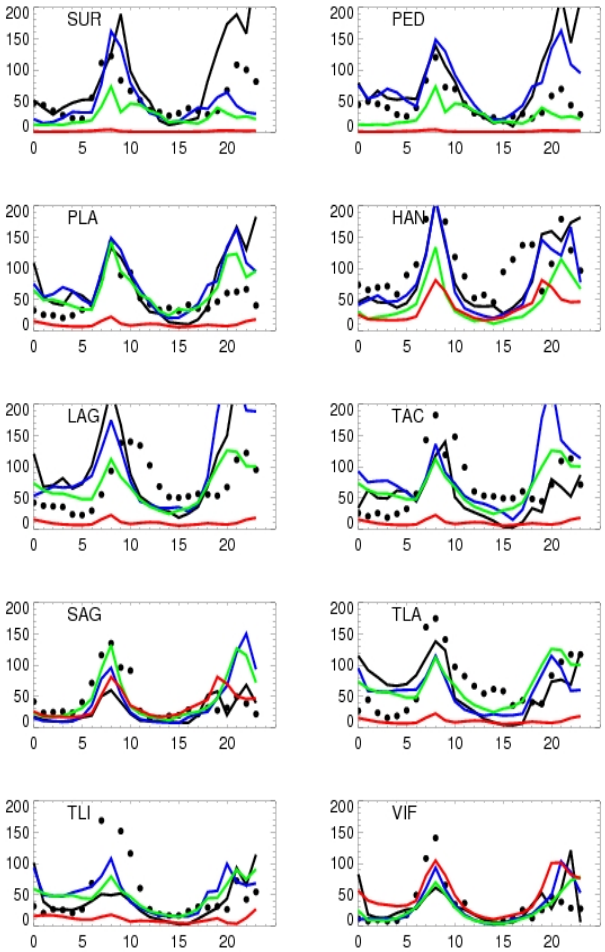

Fig. 5b. Same to Fig. 5a except for NO_x (ppbv) diurnal variations.

ACPD
10, 9801–9838, 2010

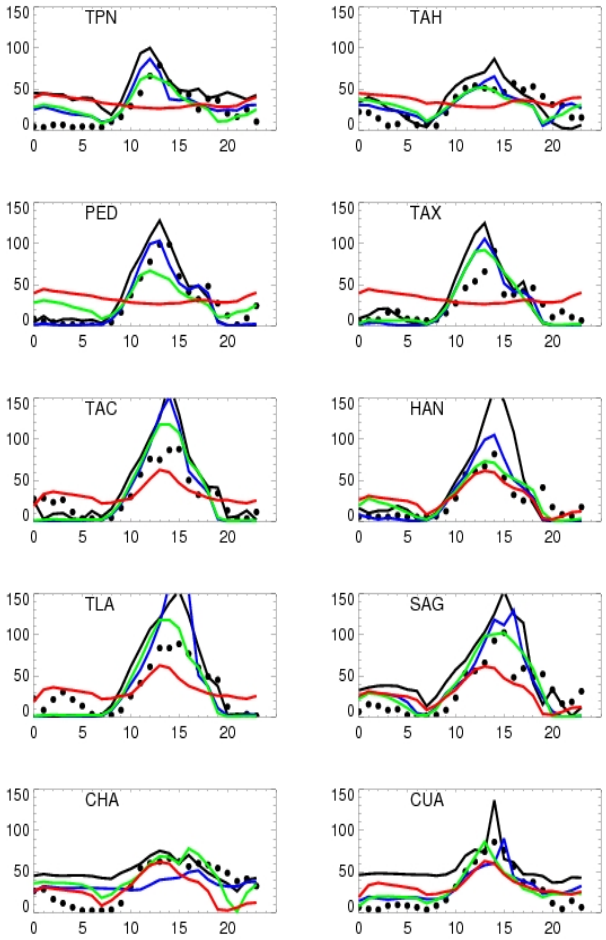

Fig. 5c. Same to Fig. 5a except for O_3 (ppbv) diurnal variations.

ACPD
10, 9801–9838, 2010

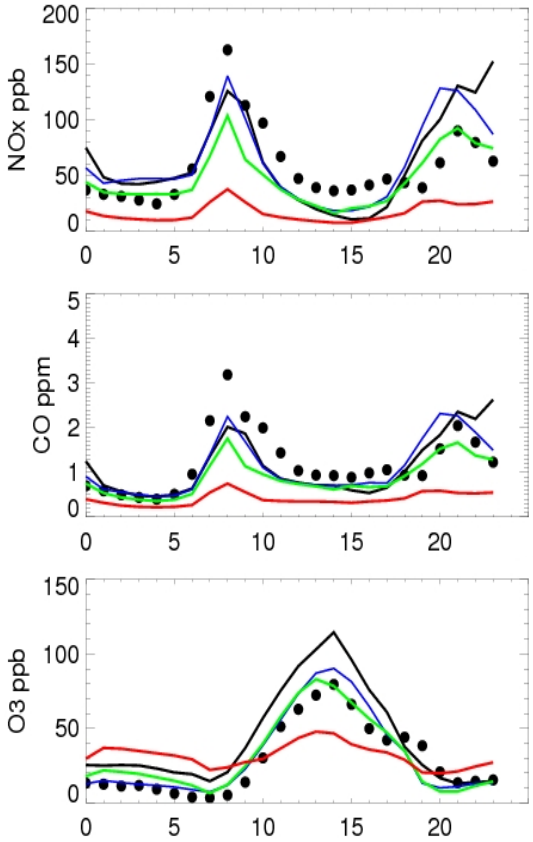

Fig. 6. Calculated and measured surface diurnal variations for NO_x (upper panel), CO (middle panel), and O_3 (lower panel). Averaged mixing ratios measured at selected sites in Mexico City. The black lines represent the calculated mixing ratios at 3 km resolution; the blue lines at 6 km resolution; the green lines at 12 km resolution, and the red lines at 24 km resolution. The black dots show the measured values.

ACPD
10, 9801–9838, 2010

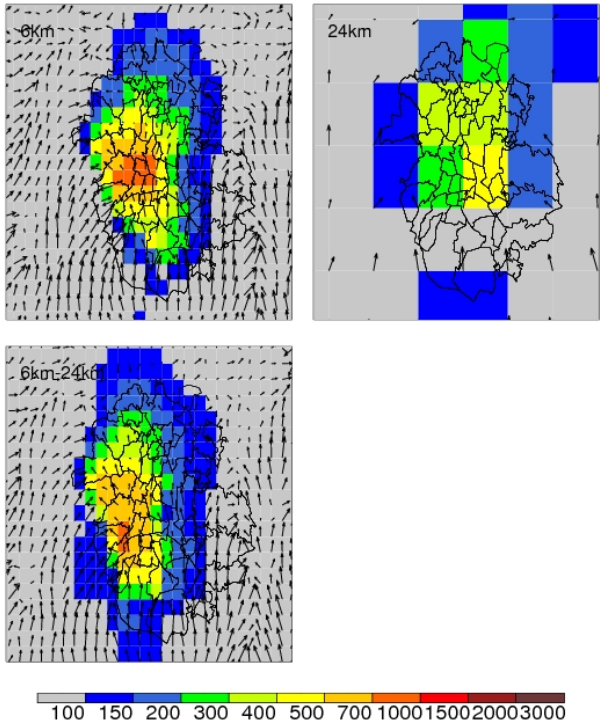

Fig. 7. Calculated surface distributions of the CO mixing ratio (ppbv) in Mexico City with wind patterns at different resolutions. Run-2 corresponds to 6 km resolution, Run-4 to 24 km resolution, and Run-5 to 6 km resolution with 24 emission resolution.

ACPD
10, 9801–9838, 2010

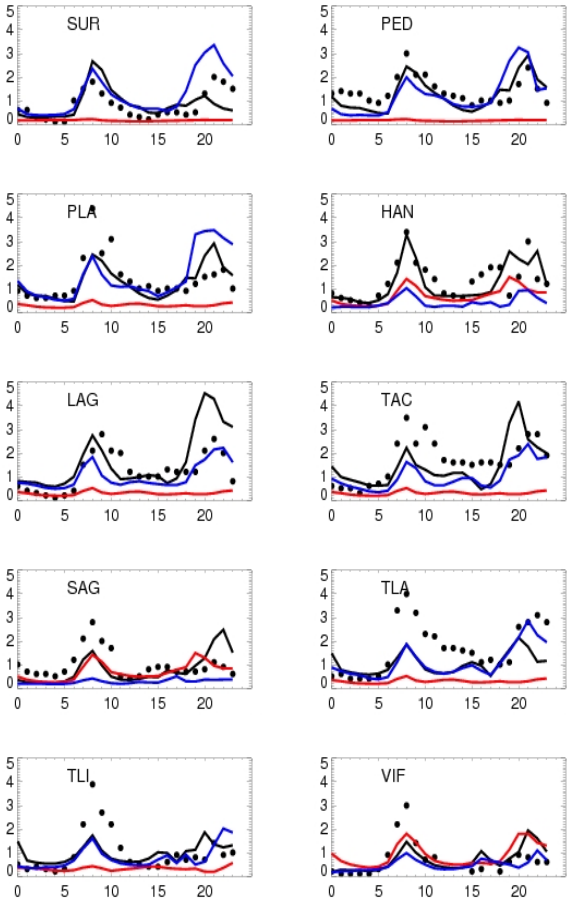

Fig. 8. Calculated and measured CO diurnal variations in the surface mixing ratio (ppmv) at different sites (shown in Table 1) for different resolutions in Mexico City. The black lines represent the mixing ratio calculated in Run-2; the blue lines represent the values calculated in Run-5; the red lines represent the values calculated in Run-4. The black dots represent the measured values.

ACPD
10, 9801–9838, 2010

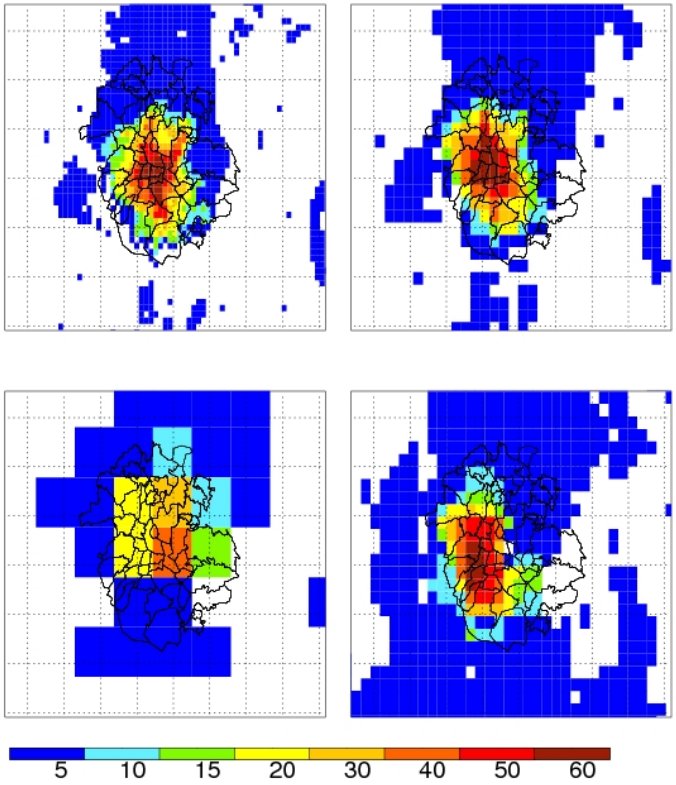

Fig. 9. Calculated surface distributions of the O_3 production rate (ppbv/hour) (see Eq. 1) in Mexico City from Run-1 (3 km resolution), Run-2 (6 km resolution), Run-4 (24 km resolution), and Run-5 (6 km resolution with 24 emission resolution).

ACPD
10, 9801–9838, 2010

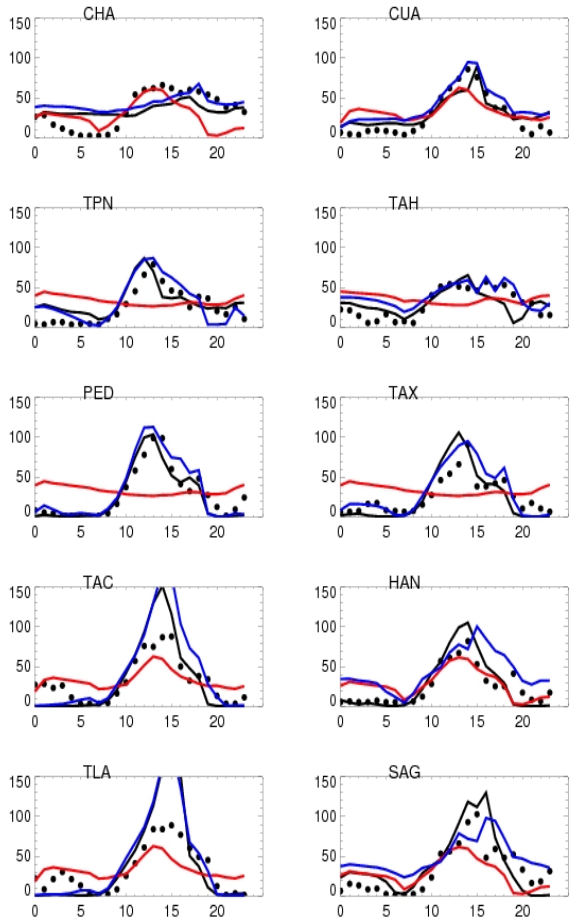

Fig. 10. Calculated and measured diurnal variations in surface ozone mixing ratio at different resolutions in Mexico City. The black lines represent the calculated mixing ratio from Run-2; the blue lines the calculated result from Run-5; the red lines the calculated result from Run-4. The black dots represent the measured values.

ACPD
10, 9801–9838, 2010

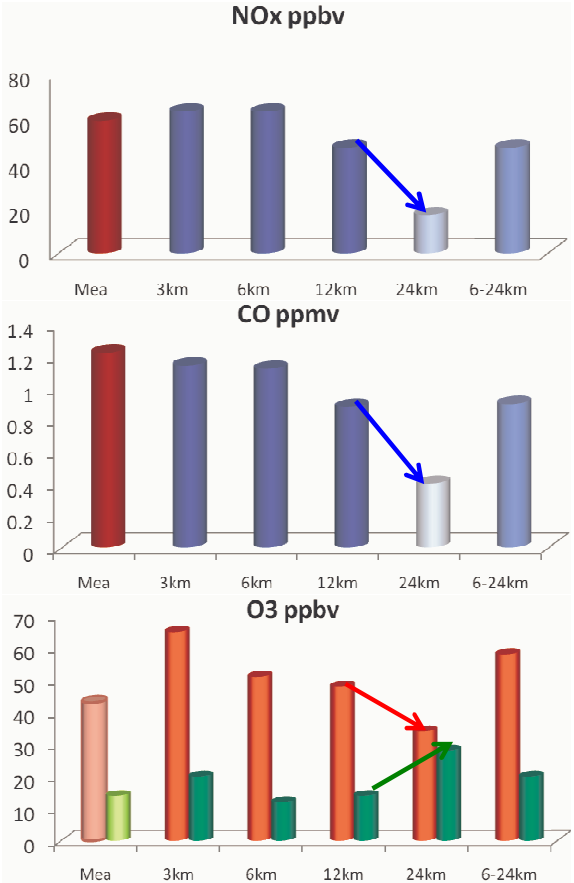

Fig. 11. Calculated and measured mean surface concentrations for NO_x (upper panel), CO (middle panel), and O_3 (lower panel) averaged at the measurement sites for different model resolutions in Mexico City. The arrows indicate the sharp change of concentrations at the threshold resolution point.

ACPD
10, 9801–9838, 2010

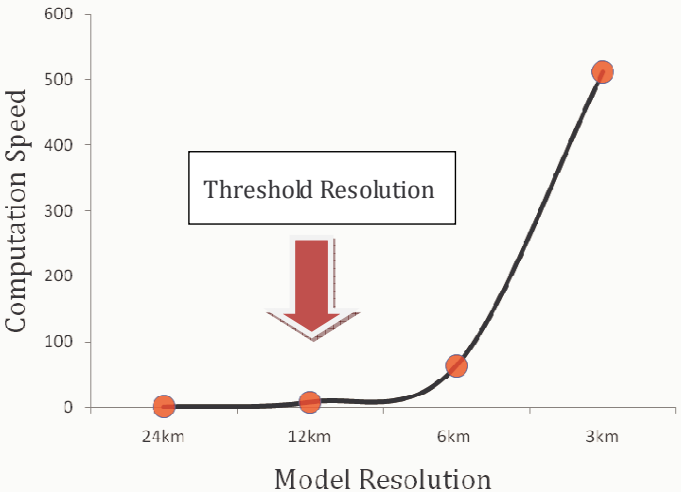

Fig. 12. Relationship between the WRF-Chem model resolution and computation time required for the each individual calculation.

ACPD
10, 9801–9838, 2010